Supplementary Material

I. MASS LOADED STRING EXAMPLE

A. Finding K and frequency through wave equation

In the limit where $l \ll L$, the frequencies of the string are well approximated by the wave equation calculation. Here, we can calculate the wavenumber of the fundamental mode by solving the equation

$$\frac{d^2u}{dx^2} + K\left(x\right)^2 u = 0, \tag{1}$$

where

$$K^2(x) = \begin{cases} \frac{\rho_m}{\sigma_0}\left(2\pi f\right)^2 & 0 \le x < a, \quad b < x \le L \\ \frac{\rho_m+\rho_M}{\sigma_0}\left(2\pi f\right)^2 & a \le x \le b \end{cases}. \tag{2}$$

The boundary conditions are given by

$$\begin{cases} u(x=0) = 0 \\ u(x=L) = 0 \\ \frac{d^n u}{dx^n} \text{ continuous at } x = a \quad n = 0, 1 \\ \frac{d^n u}{dx^n} \text{ continuous at } x = b \quad n = 0, 1 \end{cases}.$$

After using the first and second boundary conditions, the solution has the form:

$$u\left(x\right) = \begin{cases} A_1 \sin\left(\frac{\alpha}{\sqrt{1+\chi}}x\right) & 0 \le x < a \\ A_2 \sin\left(\alpha\left(x - \frac{a+b}{2}\right)\right) + B_2 \cos\left(\alpha\left(x - \frac{a+b}{2}\right)\right) & a \le x \le b \\ A_3 \sin\left(\frac{\alpha}{\sqrt{1+\chi}}\left(L-x\right)\right) & b \le x < L \end{cases}, \tag{3}$$

This is equivalent to the more compact form in the main text. As in the main text, we defined $\alpha = \sqrt{\frac{\rho_m+\rho_M}{\sigma_0}\left(2\pi f\right)^2}$. In order to find α, we can write the boundary conditions matrix equation for the coefficients A_1, A_2, B_2, A_3:

$$\begin{pmatrix} \sin\left(\frac{\alpha}{\sqrt{1+\chi}}a\right) & -\sin\left(\alpha\left(\frac{a-b}{2}\right)\right) & -\cos\left(\alpha\left(\frac{a-b}{2}\right)\right) & 0 \\ \frac{\alpha}{\sqrt{1+\chi}}\cos\left(\frac{\alpha}{\sqrt{1+\chi}}a\right) & -\alpha\cos\left(\alpha\left(\frac{a-b}{2}\right)\right) & \alpha\sin\left(\alpha\left(\frac{a-b}{2}\right)\right) & 0 \\ 0 & \sin\left(\alpha\left(\frac{b-a}{2}\right)\right) & \cos\left(\alpha\left(\frac{b-a}{2}\right)\right) & -\sin\left(\frac{\alpha}{\sqrt{1+\chi}}\left(L-b\right)\right) \\ 0 & \alpha\cos\left(\alpha\left(\frac{b-a}{2}\right)\right) & -\alpha\sin\left(\alpha\left(\frac{b-a}{2}\right)\right) & \frac{\alpha}{\sqrt{1+\chi}}\cos\left(\frac{\alpha}{\sqrt{1+\chi}}\left(L-b\right)\right) \end{pmatrix} \begin{pmatrix} A_1 \\ A_2 \\ B_2 \\ A_3 \end{pmatrix} = \begin{pmatrix} 0 \\ 0 \\ 0 \\ 0 \end{pmatrix}, \tag{4}$$

and find the α for which the determinant nulls. This results in a (typically transcendental) equation for α, and this equation was the one used to compute the frequencies in Fig. 1c in the main text.

We can further approximate and find the large mass limit of α. To do so, we can take $\sqrt{1+\chi}$ to be very large, such that $\sin\left(\frac{\alpha}{\sqrt{1+\chi}}x\right) \to \frac{\alpha}{\sqrt{1+\chi}}x$, $\cos\left(\frac{\alpha}{\sqrt{1+\chi}}x\right) \to 1$ for any $0 \le x \le L$. Note that, even though α depends on $\sqrt{1+\chi}$, $\frac{\alpha}{\sqrt{1+\chi}}$ converges to zero as $\sqrt{1+\chi}$ increases, because as the load mass increases, the frequency of the oscillator goes to zero. Because we are looking for a zero determinant, we can multiply rows and columns by a number and the zero condition would not change. The resulting matrix is

$$\begin{pmatrix} \alpha a & -\sin\left(\alpha\left(\frac{a-b}{2}\right)\right) & -\cos\left(\alpha\left(\frac{a-b}{2}\right)\right) & 0 \\ 1 & -\cos\left(\alpha\left(\frac{a-b}{2}\right)\right) & \sin\left(\alpha\left(\frac{a-b}{2}\right)\right) & 0 \\ 0 & \sin\left(\alpha\left(\frac{b-a}{2}\right)\right) & \cos\left(\alpha\left(\frac{b-a}{2}\right)\right) & -\alpha\left(L-b\right) \\ 0 & \cos\left(\alpha\left(\frac{b-a}{2}\right)\right) & -\sin\left(\alpha\left(\frac{b-a}{2}\right)\right) & 1 \end{pmatrix} \tag{5}$$

and its equation for zero determinant is:

$$\cos\left(\alpha\left(a-b\right)\right)\left[-\left(L-\left(b-a\right)\right)\alpha + \left(1 - a\left(L-b\right)\alpha^2\right)\tan\left(\left(a-b\right)\alpha\right)\right] = 0. \tag{6}$$

which yields the two sets of solutions:

$$\cos\left(\alpha\left(a-b\right)\right)=0 \tag{7}$$

$$\tan\left(\left(a-b\right)\alpha\right)=\frac{\left(L-\left(b-a\right)\right)\alpha}{\left(1-a\left(L-b\right)\alpha^{2}\right)}. \tag{8}$$

The main result from this calculation is that for a large enough load mass the equation becomes load-mass independent. Under the assumption of small mass loaded regime, i.e. $\left(b-a\right)\alpha\ll 1$, we can simplify the equation by $\tan\left(\left(a-b\right)\alpha\right)\approx\left(a-b\right)\alpha$, and the fundamental mode α in the large mass limit is then given by

$$\alpha_{\lim}=\sqrt{\frac{L}{a\left(b-a\right)\left(L-b\right)}} \tag{9}$$

B. Outline of the full string solution

Starting from Equation (4) and (5) in the main text, we can use a solution of the form:

$$u\left(x\right)=\begin{cases}A_{1}x+B_{1}+C_{1}\sinh\left(\frac{2\pi}{l}x\right)+D_{1}\cosh\left(\frac{2\pi}{l}x\right) & 0\leq x<a\\ A_{2}\sin\left(\beta_{t}x\right)+B_{2}\cos\left(\beta_{t}x\right) & \\ \qquad +C_{2}\sinh\left(\beta_{h}x\right)+D_{2}\cosh\left(\beta_{h}x\right) & a\leq x\leq b\\ A_{3}\left(x-L\right)+B_{3}+C_{3}\sinh\left(\frac{2\pi}{l}\left(x-L\right)\right)+D_{3}\cosh\left(\frac{2\pi}{l}\left(x-L\right)\right) & b<x\leq L\end{cases}, \tag{10}$$

with

$$\beta_{t}=\sqrt{\left(\frac{2\pi^{2}}{l^{2}}\right)\left(-1+\sqrt{1+4\alpha_{\lim}^{2}\left(\frac{l}{2\pi}\right)^{2}}\right)},$$

$$\beta_{h}=\sqrt{\left(\frac{2\pi^{2}}{l^{2}}\right)\left(1+\sqrt{1+4\alpha_{\lim}^{2}\left(\frac{l}{2\pi}\right)^{2}}\right)}.$$

Imposing the edge boundary conditions:

$$\begin{cases}u(x=0)=\frac{du}{dx}(x=0)=0\\ u(x=L)=\frac{du}{dx}(x=L)=0\end{cases},$$

we can simplify the solution a bit and we get:

$$u\left(x\right)=\begin{cases}A_{1}\left(x-\frac{l}{2\pi}\sinh\left(\frac{2\pi}{l}x\right)\right)+B_{1}\left(1-\cosh\left(\frac{2\pi}{l}x\right)\right) & 0\leq x<a\\ A_{2}\sin\left(\beta_{t}x\right)+B_{2}\cos\left(\beta_{t}x\right) & \\ \qquad +C_{2}\sinh\left(\beta_{h}x\right)+D_{2}\cosh\left(\beta_{h}x\right) & a\leq x\leq b\\ A_{3}\left(L-x-\frac{l}{2\pi}\sinh\left(\frac{2\pi}{l}\left(L-x\right)\right)\right) & \\ \qquad +B_{3}\left(1-\cosh\left(\frac{2\pi}{l}\left(L-x\right)\right)\right) & b<x\leq L\end{cases} \tag{11}$$

$A_i, B_i, C_i, D_i, i=1,2,3$ are coefficients determined from the boundary conditions

$$\begin{cases}\frac{d^{n}u}{dx^{n}}\text{ continuous at }x=a & n=0,1,2,3\\ \frac{d^{n}u}{dx^{n}}\text{ continuous at }x=b & n=0,1,2,3\end{cases}$$

and the initial condition.

II. MASS LOADED CIRCULAR MEMBRANE EXAMPLE

A. Statement of the problem

In this section, we show that the key ideas used in the string geometry case are general, and we apply them to another geometry example - a 2D circular membrane, with a mass load at the center.

We begin by writing the full membrane equation in 2D (corresponding to Eq. 2 in the main text):

$$\left(\frac{l}{2\pi}\right)^2\left(\frac{\partial^2}{\partial x^2}+\frac{\partial^2}{\partial y^2}\right)^2 u-\left(\frac{\partial^2}{\partial x^2}+\frac{\partial^2}{\partial y^2}\right)u-\frac{\rho\left(x,y\right)\left(2\pi f\right)^2}{\sigma_0}u=0. \tag{12}$$

Next, we rewrite it in polar coordinates:

$$\left(\frac{l}{2\pi}\right)^2\left(\frac{\partial^2}{\partial r^2}+\frac{1}{r}\frac{\partial}{\partial r}+\frac{1}{r^2}\frac{\partial^2}{\partial \theta^2}\right)^2 u-\left(\frac{\partial^2}{\partial r^2}+\frac{1}{r}\frac{\partial}{\partial r}+\frac{1}{r^2}\frac{\partial^2}{\partial \theta^2}\right)u-\frac{\rho\left(r,\theta\right)\left(2\pi f\right)^2}{\sigma_0}u=0. \tag{13}$$

for $0\leq r\leq b$, and with the boundary conditions $u\left(r=b\right)=0$. Next, for simplicity, we impose a full circular symmetry:

$$\left(\frac{l}{2\pi}\right)^2\left(\frac{\partial^2}{\partial r^2}+\frac{1}{r}\frac{\partial}{\partial r}\right)^2 u-\left(\frac{\partial^2}{\partial r^2}+\frac{1}{r}\frac{\partial}{\partial r}\right)u-\frac{\rho\left(r\right)\left(2\pi f\right)^2}{\sigma_0}u=0, \tag{14}$$

and we write the mass loading as

$$\rho\left(r\right)=\begin{cases}\rho_m+\rho_M & 0\leq r<a\\ \rho_m & a\leq r\leq b\end{cases}. \tag{15}$$

B. Showing high mass limit independence of loaded region wavenumber

Like the string case, we solve for the mode's frequency by neglecting the fourth order term in the equation. this results in a Bessel equation, which yields the solution:

$$u\left(x\right)= \tag{16}$$

$$\begin{cases}A_1 J_0\left(\alpha r\right) & 0\leq r<a\\ A_2\left(J_0\left(\frac{\alpha}{\sqrt{1+\chi}}r\right)-\left(\frac{J_0\left(\frac{\alpha}{\sqrt{1+\chi}}b\right)}{Y_0\left(\frac{\alpha}{\sqrt{1+\chi}}b\right)}\right)Y_0\left(\frac{\alpha}{\sqrt{1+\chi}}r\right)\right) & a\leq r\leq b\end{cases}, \tag{17}$$

where J_0 and Y_0 are zero order Bessel functions of the first and second kind respectively, and like in the main text, we defined the wavenumber in the loaded regime $\alpha=2\pi f\sqrt{\frac{\rho_m+\rho_M}{\sigma_0}}$, using $\chi=\frac{\rho_M}{\rho_m}$, and where we already used the solution continuity at $r=0$ and the boundary condition at $r=b$.

The remaining boundary conditions at $r=a$ can be represented as a matrix equation:

$$\begin{pmatrix} J_0\left(\alpha a\right) & -J_0\left(\frac{\alpha}{\sqrt{1+\chi}}a\right)+\left(\frac{J_0\left(\frac{\alpha}{\sqrt{1+\chi}}b\right)}{Y_0\left(\frac{\alpha}{\sqrt{1+\chi}}b\right)}\right)Y_0\left(\frac{\alpha}{\sqrt{1+\chi}}a\right)\\ -\alpha J_1\left(\alpha a\right) & \frac{\alpha}{\sqrt{1+\chi}}J_1\left(\frac{\alpha}{\sqrt{1+\chi}}a\right)-\frac{\alpha}{\sqrt{1+\chi}}\left(\frac{J_0\left(\frac{\alpha}{\sqrt{1+\chi}}b\right)}{Y_0\left(\frac{\alpha}{\sqrt{1+\chi}}b\right)}\right)Y_1\left(\frac{\alpha}{\sqrt{1+\chi}}a\right)\end{pmatrix}\begin{pmatrix}A_1\\A_2\end{pmatrix}=\begin{pmatrix}0\\0\end{pmatrix}, \tag{18}$$

which is satisfied with a non-trivial solution when the matrix determinant nulls. The equation

$$\left|\begin{pmatrix} J_0(\alpha a) & -J_0\left(\frac{\alpha}{\sqrt{1+\chi}}a\right)+\left(\frac{J_0\left(\frac{\alpha}{\sqrt{1+\chi}}b\right)}{Y_0\left(\frac{\alpha}{\sqrt{1+\chi}}b\right)}\right)Y_0\left(\frac{\alpha}{\sqrt{1+\chi}}a\right) \\ -\alpha J_1(\alpha a) & \frac{\alpha}{\sqrt{1+\chi}}J_1\left(\frac{\alpha}{\sqrt{1+\chi}}a\right)-\frac{\alpha}{\sqrt{1+\chi}}\left(\frac{J_0\left(\frac{\alpha}{\sqrt{1+\chi}}b\right)}{Y_0\left(\frac{\alpha}{\sqrt{1+\chi}}b\right)}\right)Y_1\left(\frac{\alpha}{\sqrt{1+\chi}}a\right) \end{pmatrix}\right|=0, \tag{19}$$

where $|\cdot|$ denotes taking determinant, is therefore an equation for α that satisfies the boundary conditions.
We now show that at the limit of large density ratio χ, this equation becomes independent of χ. In order to do that, we use the asymptotic behavior of some of the function in the matrix element for small arguments:

$$\begin{cases} J_0\left(\frac{\alpha}{\sqrt{1+\chi}}a\right)\to 1, & J_0\left(\frac{\alpha}{\sqrt{1+\chi}}b\right)\to 1 \\ Y_0\left(\frac{\alpha}{\sqrt{1+\chi}}a\right)\to\frac{2}{\pi}\left[\log\left(\frac{\alpha}{2\sqrt{1+\chi}}a\right)+\gamma\right], & Y_0\left(\frac{\alpha}{\sqrt{1+\chi}}b\right)\to\frac{2}{\pi}\left[\log\left(\frac{\alpha}{2\sqrt{1+\chi}}b\right)+\gamma\right] \\ Y_1\left(\frac{\alpha}{\sqrt{1+\chi}}a\right)\to-\frac{1}{\pi}\left(\frac{2}{\frac{\alpha}{\sqrt{1+\chi}}a}\right) & \\ J_1\left(\frac{\alpha}{\sqrt{1+\chi}}a\right)\to\left(\frac{\alpha}{2\sqrt{1+\chi}}a\right) & \end{cases}, \tag{20}$$

where γ is a mathematical constant related to the bessel function of the second kind. Using these asymptotic approximations, we can write our equation for large χ as:

$$\left|\begin{pmatrix} J_0(\alpha a) & -\frac{\log\left(\frac{b}{a}\right)}{\log\left(\frac{\alpha}{2\sqrt{1+\chi}}b\right)+\gamma} \\ -\alpha J_1(\alpha a) & \left(\left(\frac{\alpha}{\sqrt{1+\chi}}\right)^2\frac{a}{2}+\left(\frac{\left(\frac{1}{a}\right)}{\log\left(\frac{\alpha}{2\sqrt{1+\chi}}b\right)+\gamma}\right)\right) \end{pmatrix}\right|=0. \tag{21}$$

Now, as we did in the string case, multiplying the right column of the matrix by a number does not change the solution of the equation. Therefore, we can multiply the right column by $\log\left(\frac{\alpha}{2\sqrt{1+\chi}}b\right)+\gamma$, and we get:

$$\left|\begin{pmatrix} J_0(\alpha a) & -\log\left(\frac{b}{a}\right) \\ -\alpha J_1(\alpha a) & \left(\frac{\alpha}{\sqrt{1+\chi}}\right)^2\frac{a}{2}\left(\log\left(\frac{\alpha}{2\sqrt{1+\chi}}b\right)+\gamma\right)+\left(\frac{1}{a}\right) \end{pmatrix}\right|=0. \tag{22}$$

Now, taking the limit of large χ, or $\frac{\alpha}{\sqrt{1+\chi}}\to 0$, we get the final large-mass-limit equation for α:

$$\left|\begin{pmatrix} J_0(\alpha a) & -\log\left(\frac{b}{a}\right) \\ -\alpha J_1(\alpha a) & \left(\frac{1}{a}\right) \end{pmatrix}\right|=0\Rightarrow J_0(\alpha a)=\alpha a J_1(\alpha a)\log\left(\frac{b}{a}\right) \tag{23}$$

which is independent of the mass ratio χ. We can again denote the solution for the fundamental mode of this equation as $\alpha_{\lim}$. A comparison between the above calculation and a FEA simulation for a membrane is presented in Fig. 1. Here, we chose $b=500\,\mu$m, $a=5\,\mu$m.

C. Solution outline and general form

We can now write the large mass limit membrane equation for the fundamental mode:

$$\left(\frac{l}{2\pi}\right)^2\left(\frac{\partial^2}{\partial r^2}+\frac{1}{r}\frac{\partial}{\partial r}\right)^2 u-\left(\frac{\partial^2}{\partial r^2}+\frac{1}{r}\frac{\partial}{\partial r}\right)u-K(r)^2 u=0, \tag{24}$$

where

$$K(r)^2=\begin{cases}\alpha_{\lim}^2 & 0\le r<a \\ 0 & a\le r\le b\end{cases}. \tag{25}$$

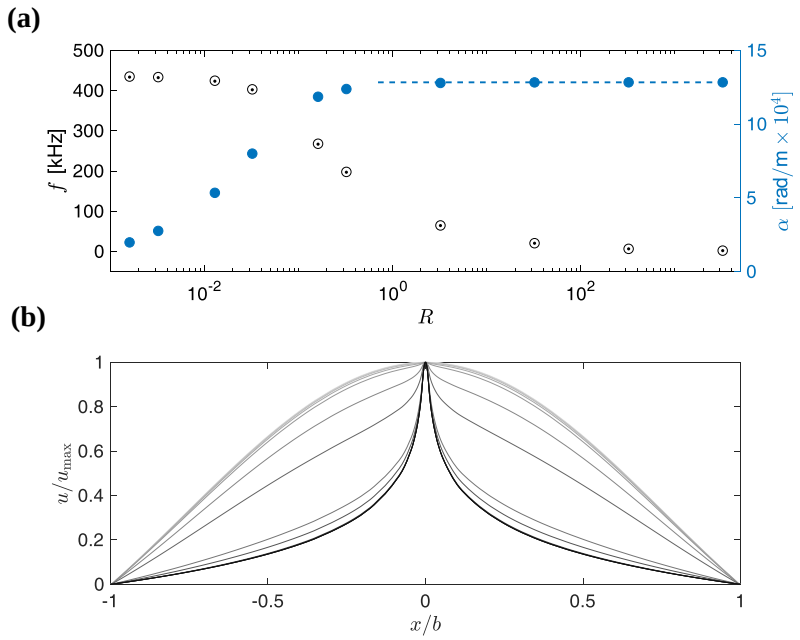

FIG. 1. **Mode saturation for a mass loaded circular membrane. (a)** Comparison between analytical model and FEA calculation for a mass-loaded circular membrane. The analytically calculated membrane frequencies (black dots) are in good agreement with the FEA simulated frequencies (empty black circles) as a function of R, defined as the ratio between the load mass and the total unloaded resonator mass. The calculated mass-loaded regime wavenumber α (blue full circles) exhibits an obvious saturation, which agrees with the limit calculated from the analytical model, α_{lim} (dashed blue line). **(b)** Normalized mode shape visualization, for different load mass. Here, x denotes the displacement from the membrane center, along a line passing through the center. Lighter shades of grey correspond to lighter load mass. The mode shapes correspond to the points in (a).

Solving for $a \leq r \leq b$, we rewrite the equation as:

$$\left(\frac{\partial^2}{\partial r^2}+\frac{1}{r}\frac{\partial}{\partial r}\right)\left[\left(\frac{l}{2\pi}\right)^2\left(\frac{\partial^2}{\partial r^2}+\frac{1}{r}\frac{\partial}{\partial r}\right)-1\right]u=0, \tag{26}$$

which can be solved by splitting it into two parts, each provides a solution with two degrees of freedom:

$$\left(\frac{\partial^2}{\partial r^2}+\frac{1}{r}\frac{\partial}{\partial r}\right)u=0\Rightarrow u\left(r\right)=A\ln\left(\frac{r}{B}\right), \tag{27}$$

and

$$\left[\left(\frac{\partial^2}{\partial\left(\frac{2\pi}{l}r\right)^2}+\frac{1}{\frac{2\pi}{l}r}\frac{\partial}{\partial\left(\frac{2\pi}{l}r\right)}\right)-1\right]u=0\Rightarrow u\left(r\right)=CI_0\left(\frac{2\pi}{l}r\right)+DK_0\left(\frac{2\pi}{l}r\right), \tag{28}$$

where $I_0\left(\cdot\right)$ and $K_0\left(\cdot\right)$ are the zeroth order modified Bessel functions of the first and second kind, respectively. The solution for the $a \leq r \leq b$ regime is therefore:

$$u\left(r\right)=A\ln\left(\frac{r}{B}\right)+CI_0\left(\frac{2\pi}{l}r\right)+DK_0\left(\frac{2\pi}{l}r\right). \tag{29}$$

Solving for the region $r < a$, we can write our equation as:

$$\left[\frac{1}{\eta_h^2}\left(\frac{\partial^2}{\partial r^2}+\frac{1}{r}\frac{\partial}{\partial r}\right)-1\right]\left[\frac{1}{\eta_t^2}\left(\frac{\partial^2}{\partial r^2}+\frac{1}{r}\frac{\partial}{\partial r}\right)+1\right]U=0, \tag{30}$$

where

$$\eta_t = \sqrt{\left(\frac{2\pi^2}{l^2}\right)\left(-1+\sqrt{1+4\alpha_{\text{lim}}^2\left(\frac{l}{2\pi}\right)^2}\right)},$$

$$\eta_h = \sqrt{\left(\frac{2\pi^2}{l^2}\right)\left(1+\sqrt{1+4\alpha_{\text{lim}}^2\left(\frac{l}{2\pi}\right)^2}\right)}.$$

This in turn, provides a general solution in the form of:

$$u(r) = AY_0(\eta_t r) + BJ_0(\eta_t r) + CI_0(\eta_t r) + DK_0(\eta_t r). \tag{31}$$

Taking into account continuity at the center, we conclude that the full solution has to be of the form:

$$u(r) = \begin{cases} A_1 \ln\left(\frac{r}{B_1}\right) + C_1 I_0\left(\frac{2\pi}{l}r\right) + D_1 K_0\left(\frac{2\pi}{l}r\right) & a \le r \le b \\ B_2 J_0(\eta_t r) + C_2 I_0(\eta_t r) & r < a \end{cases} \tag{32}$$

III. FEA SIMULATIONS

We performed FEA simulations on COMSOL Multiphysics (software version 5.6) to find the expected resonator mode frequencies and Q values. After setting up the computer-aided design (CAD) model of our resonator geometry along with the relevant material properties, boundary conditions, initial conditions, and mesh, we used COMSOL's Solid Mechanics Module to perform a stationary study and find the stress re-distribution. The results of this were fed into an eigenfrequency study to obtain the resonator mode shapes and frequencies. The mode shape data was then post-processed to calculate the Q values. To validate the results, at the end of each simulation, we performed a mesh convergence study by systematically refining the mesh on our geometry until the resonator mode frequencies and Q values changed by a negligible amount (less than 2% and 10% respectively). For all the simulations, the calculated Q was based only on the bending loss inside material(s), and we ignored radiation loss.

In the subsections below, we discuss the details of each individual simulation that we performed and link them to figures displayed in the main text.

A. Mass loaded string

We simulated a mass loaded string to find the fundamental mode frequencies and Q_{bend} values. The results obtained from this simulation were used to create parts of Fig. 1 in the main text. The CAD model of the geometry matches what is shown in Fig. 1a of the main text. We set up the problem as a doubly-clamped string with length $L = 1$ mm, width $w = 5$ μm, thickness $h = 110$ nm. For the mass loaded region we let $b - a = 10$ μm and placed it at the center of the string. The geometry was partitioned into the inner and outer regions (defined in the main text). The film pre-patterning stress was set to a uniform value $\sigma_p = 1$ GPa (note that this is different from the re-distributed stress σ_0). The material of the entire string was set to stoichiometric silicon nitride (SiN) with density $\rho_m = 3100$ kg/m^3, Young's modulus $E = 250$ GPa, and Poisson's ratio $\nu = 0.23$. However, we changed the density of the inner region to be $\rho_m + \rho_M$ where ρ_M can be varied. We swept the value of ρ_M over a range to change the mass load. We then computed the mode shapes and frequencies from our FEA simulation. The results were used to obtain the following quantities for different mass loads: mode shape line cuts in Fig. 1b, mode frequencies (solid black circles) in Fig. 1c, mode wavenumbers (solid blue circles) in Fig. 1c, and mode quality factors (solid black circles) in Fig. 1d. When computing the quality factors the bending loss contributions from the mode edge were ignored to focus on the main mass loading effect. The computed quality factors were normalized by the quality factor of the mode without a mass load as this gives us a dimensionless geometric parameter which does not depend on the material properties being used, and it allows us to study the effect of mass loading. As a note, when meshing the geometry, for the solutions to converge, we had to use a finer mesh around the clamped edges of the string and the mass loaded region to capture the bending accurately. Finally, we clarify that all simulations done were for the fundamental mode of the string and their purpose was to validate our analytical model.

B. Mass loaded circular membrane

We simulated a mass loaded circular membrane to find the fundamental mode shapes, wavenumbers and frequencies. The results obtained from this simulation were used to create parts of Fig. 1 in the supplementary material. The geometric setup of the problem is described above in section II A of the supplementary material. We used $a = 5$ μm and $b = 500$ μm for the mass loaded membrane. The film pre-patterning stress was set to a uniform value $\sigma_p = 1$ GPa (note that this is different from the re-distributed stress σ_0). The material of the entire membrane was set to stoichiometric silicon nitride (SiN) with density $\rho_m = 3100$ kg/m^3, Young's modulus $E = 250$ GPa, and Poisson's ratio $\nu = 0.23$. However, we changed the density of the inner region to be $\rho_m + \rho_M$ where ρ_M can be varied. We swept the value of ρ_M over a range to change the mass load. We then computed the mode shapes and frequencies from our FEA simulation. The results were used to obtain the following quantities for different mass loads: mode frequencies (empty black circles) and mode inner region wavenumbers (solid blue circles) in Fig. 1a of the supplementary material, and mode shapes in Fig. 1b of the supplementary material. As a note, when meshing the geometry, for the solutions to converge, we had to use a finer mesh around the clamped edges of the membrane and the mass loaded region to capture the bending accurately. Finally, we clarify that all simulations done were for the fundamental mode of the membrane and their purpose was to validate our analytical model.

C. Trampoline resonator without mass loading

We next simulated a trampoline resonator without a mass load. The results obtained from this simulation were used to create certain parts of Fig. 3 in the main text. The overall trampoline geometry used for the simulations is shown in Fig. 2a of the main text. We used experimental data for the frequency of the fundamental mode of multiple devices to set the pre-patterning stress in our COMSOL simulation. We found that $\sigma_p = 1.007$ GPa gave good agreement between experimental and simulated frequencies for the fundamental mode. To model the SiN we used $\rho = 3100$ kg/m^3 for the density, $E = 250$ GPa for the Young's Modulus, and $\nu = 0.23$ for the Poisson's Ratio.

When computing the Q_{bend} we considered bending loss in the SiN (as explained in the main text) and used Eq. 1 from the main text after some simplification. We assumed that our devices were thin-films (h is small compared to the other dimensions of the resonator) which means that the bending loss is dominated by loss at the surface of the SiN, and this is indicated by E_2 being a function of z [1]. Under this assumption it can be shown that Eq. 1 from the main text simplifies to the following expression [2], which can then be used:

$$Q_{\text{bend}-\text{SiN}}(u) = \left(\frac{24(1-\nu^2)Q_{\text{intrinsic}-\text{SiN}}}{h^3 E}\right) \frac{W}{\int_S \left[\frac{\partial^2 u}{\partial x^2} + \frac{\partial^2 u}{\partial y^2}\right]^2 dA} \tag{33}$$

where $W \approx \int_V (\frac{\sigma_0}{2}) \left[\left(\frac{\partial u}{\partial x}\right)^2 + \left(\frac{\partial u}{\partial y}\right)^2\right] dV$ is the energy stored in the mode, S is the surface domain of the SiN resonator, and dA is an infinitesimal surface area element. It is common practice to define $Q_{\text{intrinsic}} = E/E_2$ where $Q_{\text{intrinsic}}$ is the intrinsic quality factor of a material. The value of $Q_{\text{intrinsic}-\text{SiN}}$ is variable, it depends on the specific batch of SiN used [3]. In our experiment, we mounted the trampoline device on a custom-made silicon base to minimize radiation loss. We then measured the Q_{fund} without a mass load. The value of $Q_{\text{intrinsic}-\text{SiN}}$ was estimated by fitting the highest experimentally measured Q_{fund} without a mass load, shown as an open black circle in Fig. 3a in the main text, to the simulation results. This corresponded to $Q_{\text{fund}} = 33.0 \cdot 10^6$ and it gave us $Q_{\text{intrinsic}-\text{SiN}} \approx 12959$ for a SiN thickness of 110 nm at a temperature of 300 K. This is a reasonable estimate for $Q_{\text{intrinsic}-\text{SiN}}$ and indeed it affirms that our mounting setup minimized radiation loss for the trampoline fundamental mode without mass loading. It should be noted that while meshing the geometry for this simulation, for the solutions to converge, we had to pay special attention to the mesh at the edges and fillets of the trampoline device where the losses are significant.

D. Trampoline resonator with mass loading

To study mass loading, we modified the simulations described in Subsec. III C by including a mass along with some epoxy on our trampoline resonator. We modeled the epoxy by using a small cuboid shaped slab with side length l_g and thickness t_g and we embedded a sphere of radius r_{mag} in it to model the magnetic grain. It should be noted that we did not apply pre-patterning stress on the epoxy and the magnet. The epoxy used had density $\rho = 1290$ kg/m^3, Young's modulus $E = 2.21$ GPa, and Poisson's ratio $\nu = 0.29$. We modeled magnets used in the experiment with density $\rho = 7500$ kg/m^3, Young's modulus $E = 160$ GPa, and Poisson's ratio $\nu = 0.24$. Ideally, to change the load

mass in the simulation, one would vary the sphere radius $r_{\rm mag}$. However, we chose to use a fixed value of r_{mag} and scanned the density of the magnet so as to vary the load mass. This was done to avoid nonphysical torsional mode effects that show up due to mesh asymmetry when using very large values of $r_{\rm mag}$. In our simulation, we used a relatively small radius $r_{\rm mag} = 3$ μm and scanned the density of the magnet grain domain over different values to simulate a variety of mass loads.

To compute the Q of the mass loaded modes, we looked at two different scenarios: (a) disregarding loss inside the epoxy (b) including loss inside the epoxy. Additionally for both these cases, we ignored bending loss in the magnet since we expected it to be negligibly small.

For the first case, (a), we simply used Eq. 33 to compute the Q for different mass loads. It should be noted that the stored tensile energy approximation for W mentioned earlier is challenging to calculate on COMSOL. So we used $W = 2\pi^2 f^2 \int_V \rho u^2 dV$ to find the maximum kinetic energy (this is equal to the stored tensile energy). This simulation gave rise to the theory points represented by the green dotted line on Fig. 3a.

In order to model loss inside the epoxy, (b), we used the most general formulation of bending loss which does not assume high-stress or dominant surface loss [4]. Further, it includes mechanical loss due to three dimensional deformation. With this, we obtained the following expression for the Q of the epoxy domain as:

$$Q_{\rm bend-epoxy}(u) = \left(\frac{2Q_{\rm intrinsic-epoxy}}{E}\right) \frac{W}{\int_{\rm epoxy} \left(\sum_{ij} (\epsilon_{ij})^2\right) dV} \tag{34}$$

where ϵ_{ij} is the ijth matrix element of the three dimensional spatially dependent strain tensor. We note that here we assume an isotropic value for E_2 where $E_2 = Q_{\rm intrinsic}/E$.

The Q of the SiN was found using Eq. 33 as before. The Q of the epoxy domain was found using Eq. 34. At the end, we found the overall mode Q by adding the Q values of the epoxy and SiN domains reciprocally. Based on surface tension arguments and additional simulations, we were able to conclude that the glue thickness $l_t \approx 0.8$ μm. So we scanned the values of $Q_{\rm intrinsic-epoxy}$ and the epoxy side length l_g to find that $Q_{\rm intrinsic-epoxy} \approx 20$ and $l_g \approx 4$ μm (which are both very realistic parameters) matched our experimental data the best while also providing an upper bound on the Q values. This simulation gave rise to the theory points represented by the black dotted line on Fig. 3a in the main text. It should be noted that while meshing the geometry for this simulation, for the solutions to converge, we had to pay special attention to the mesh at the edges and filets of the trampoline device, the mesh surrounding the mass loaded region, and the mesh inside the epoxy.

IV. Q AND FREQUENCY MEASUREMENTS

To readout the mechanical motion we used an etalon interferometer with infra-red laser light of wavelength $\lambda = 1064$ nm. The mode frequencies were found by identifying peaks on the measured power spectrum. To find the mode Q values, we performed ringdown measurements by driving the resonator at the mode frequencies using a piezo-electric drive. The entire experiment was conducted in a high-vacuum environment ($P < 10^{-7}$ Torr) to prevent gas damping.

V. MAGNET DEPOSITION

We deposited magnets onto our trampoline resonators inside a cleanroom. This was done under a microscope using an objective lens with a magnification of 50x. Tapered glass micropipettes (Product ID: Origio MAH-SM-0) attached to a micromanipulator were used to carefully apply ultra-violet (UV) epoxy (Product ID: NEA 123SHGA) and deposit NeFeB magnets (Product ID: Neo Magnequech MQFP-B+ (D50=25m)) on to our devices. The epoxy was cured using a UV flashlight. To perform magnetic stacking, we magnetized the grain(s) on our trampoline by using a strong electromagnet ($B > 1$ T). Although this field does not magnetically-saturate the grain(s), it is strong enough so as to allow us to perform magnetic stacking successfully.

VI. MICROFABRICATION DETAILS

The trampoline devices were fabricated on a 375 μm thick, 3 inch diameter silicon wafer with 110 nm of stoichiometric LPCVD SiN on either side. The SiN film had a pre-patterning tensile stress of roughly 1 GPa. The resonator geometry and backside windows were patterned using a direct write photolithography method. Patterning of the SiN was completed via a CF_4 reactive ion etch. The wafer was then cleaned with O_2 plasma followed by ultrasound cleaning in an acetone bath. Additional cleaning was performed with isopropyl alcohol and water. To release the

SiN structures, the window side of the wafer was etched using a 80 C KOH bath. Following wet etching, the wafer was cleaned in a Nanostrip bath, followed by a solvent clean. Devices were then left to air dry. The fully fabricated trampoline resonators had a side length of 1 mm, a tether width of 5 μm, and a pad area of approximately 86 μm^2 (Fig. 2a). An unloaded fundamental mode frequency of $\approx$ 143 kHz was measured.

VII. ADDITIONAL DETAILS ON MASS LOADED TRAMPOLINES

In this section, we go over some additional details with regards to mass loaded trampoline resonators. To be specific, we discuss how the fundamental mode $Q_{\rm bend}$ is affected by (a) the location of the mass load on the resonator and (b) the film thickness of the resonator.

A. Effect of mass loading location on trampoline $Q_{\rm bend}$

FEA simulations reveal that, for a trampoline resonator with a high mass load, the saturated $Q_{\rm bend}$ value depends on the location of mass loading. In particular, we find that the $Q_{\rm bend}$ saturates to a higher value when the mass load is on a tether rather than the trampoline pad. Further, we find the optimal location for mass loading to be the tether region near the trampoline pad. As a clarification, when calculating these results, we disregarded loss inside the epoxy and only considered loss in the SiN. The results are summarized in Fig. 2 of the supplementary material.

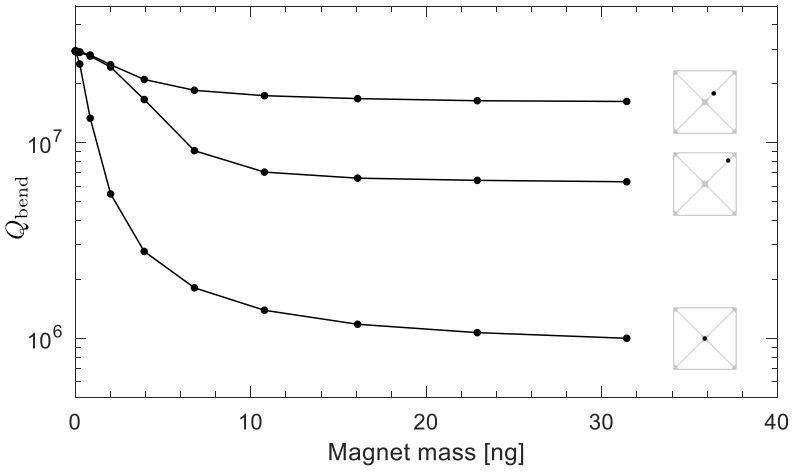

FIG. 2. **Trampoline $Q_{\rm bend}$ as a function of magnet mass and location:** The plots show $Q_{\rm bend}$ for trampolines as a function of the magnet mass and location (solid black circles with black lines). The insets (small trampolines marked with a black circle) indicate the location of the mass load in each case. For each of the three curves, the solid black circles represent FEA simulation data, and we have drawn a line joining them to indicate the general trend with increasing mass load.

B. Effect of SiN thickness on trampoline $Q_{\rm bend}$

It is known that for soft clamped resonators $Q_{\rm bend} \propto h^{-1}$ [1, 2] and because trampolines can be considered as partially soft-clamped resonators, we expect that $Q_{\rm bend}$ reduces with increasing thickness. However, when a mass load is present we find the situation is more complicated. For small masses the mode shape barely changes, and in this situation, as expected, thinner SiN offers the best $Q_{\rm bend}$ values. But as the mass increases, we observe a transition in the trend, and surprisingly, for intermediate masses, thicker SiN leads to the highest $Q_{\rm bend}$ values. However, in the limit of a large mass load, thinner SiN leads to the highest $Q_{\rm bend}$ values. But in this regime, it appears that $Q_{\rm bend}$ saturates to approximately the same value irrespective of the SiN thickness. Once again, when calculating these results, to clarify, we disregarded loss inside the epoxy and only included bending loss in the SiN. The results are illustrated in Fig. 3 of the supplementary material.

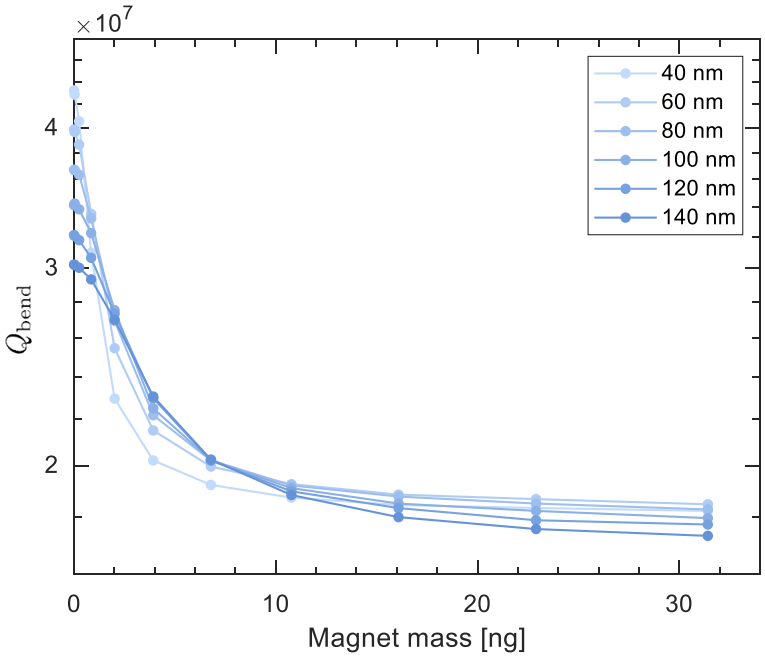

FIG. 3. Q_{bend} **as a function of magnet mass for different SiN thicknesses:** The plots show Q_{bend} as a function of magnet mass for different SiN thicknesses (colored blue circles with colored blue lines). The legend (top right) indicates the nitride thickness (the lightest shade of blue corresponds to the thinnest SiN while the darkest corresponds to the thickest). For each of the curves, the solid points represent simulation data, and we have drawn a line joining them to indicate the general trend with increasing mass load.

[1] Tsaturyan, Y., Barg, A., Polzik, E. & Schliesser, A. Ultracoherent nanomechanical resonators via soft clamping and dissipation dilution. *Nature Nanotechnology*. **12**, 776-783 (2017)
[2] Reetz, C., Fischer, R., Assumpcao, G., McNally, D., Burns, P., Sankey, J. & Regal, C. Analysis of membrane phononic crystals with wide band gaps and low-mass defects. *Physical Review Applied*. **12**, 044027 (2019)
[3] Villanueva, L. & Schmid, S. Evidence of surface loss as ubiquitous limiting damping mechanism in SiN micro-and nanomechanical resonators. *Physical Review Letters*. **113**, 227201 (2014)
[4] LD, L. & LIFSHITZ, E. Course of theoretical physics. Theory Of Elasticity. (Pergamon,1975)